Prediction of resilient modulus of ballast under cyclic loading using machine learning techniques

Buddhima Indraratna, PhD (Alberta), FIEAust., FTSE, FASCE

Distinguished Professor of Civil Engineering and Director of Transport Research Centre, University of Technology Sydney, Ultimo, Australia

Danial Jahed Armaghani, PhD

Research Fellow, Transport Research Centre, School of Civil and Environmental Engineering, University of Technology Sydney, Ultimo, Australia.

António Gomes Correia, PhD

Professor of Civil Engineering, Department of Civil Engineering, ISISE, University of Minho, Campus de Azurém, 4800-058, Guimarães, Portugal.

Haydn Hunt, PhD student

Transport Research Centre, School of Civil and Environmental Engineering, University of Technology Sydney, Ultimo, Australia.

Trung Ngo, PhD, CPEng, M.ASCE

Senior lecturer, Transport Research Centre, School of Civil and Environmental Engineering, University of Technology Sydney, Ultimo, Australia.

Original article: Submitted to Transportation Geotechnics

Author for correspondence:

Distinguished Professor B. Indraratna

Faculty of Engineering and Information Technology

University of Technology Sydney

Ultimo, NSW 2007

Australia.

Ph: +61 2 9514 8000

Email: buddhima.indraratna@uts.edu.au

Prediction of resilient modulus of ballast under cyclic loading using machine learning techniques

Buddhima Indraratna[1], Danial Jahed Armaghani[2], António Gomes Correia[3], Haydn Hunt[4], Trung Ngo[5]

[1]Distinguished Professor of Civil Engineering and Director of Transport Research Centre, University of Technology Sydney, Ultimo, Australia. Email: buddhima.indraratna@uts.edu.au

[2]Research Fellow, Transport Research Centre, School of Civil and Environmental Engineering, University of Technology Sydney, Ultimo, Australia. Email: danial.jahedarmaghani@uts.edu.au

[3] Professor of Civil Engineering, Department of Civil Engineering, ISISE, University of Minho, Campus de Azurém, 4800-058, Guimarães, Portugal. Email: agc@civil.uminho.pt

[4]PhD Student, Transport Research Centre, School of Civil and Environmental Engineering, University of Technology Sydney, Ultimo, Australia. Email: Haydn.R.Hunt@student.uts.edu.au

[5]Senior Lecturer, Transport Research Centre, School of Civil and Environmental Engineering, University of Technology Sydney, Ultimo, Australia. Email: Trung.Ngo@uts.edu.au

Abstract:

The resilient modulus (M_R) of ballast is one of the key output parameters in any rail design project because it controls the elastic magnitude of track deformation under cyclic loading. This study investigates the response of M_R under cyclic conditions as a function of four key parameters, i.e., the loading magnitude, the number of loading cycles, the loading frequency, and the confining pressure. To do so, two non-linear predictive models, namely, the artificial neural network (ANN), and the adaptive neuro-fuzzy inference system (ANFIS), are used to predict the M_R values under different loading conditions. To evaluate and predict M_R, an experimental database with 196 data samples is considered in this study. A series of sensitivity analyses is carried out to investigate the most effective parameters in each non-linear model and also predict the highest performance model. Although the results from the primary validation phase are satisfactory for the ANN and ANFIS models, ANFIS proves better (i.e., the coefficient of determination = 0.709) at estimating the M_R during the secondary validation phase, using an independent dataset. Hence, it can be used as a powerful and practical model for predicting the magnitude of M_R. On the basis of the ANFIS model, this study also offers

some design considerations in terms of M_R of ballast under a practical range of cyclic loading parameters.

Keywords: *Railway geotechnics; Ballast; Resilient modulus; Predictive models; Cyclic loading; Machine learning.*

Nomenclature

ANN	Artificial neural network
ANFIS	Adaptive neuro-fuzzy inference system
AI	Artificial intelligence
BP	Back-propagation
$\emptyset$	Bulk stress
C	Percentage of clay
D	The total number of data samples
σ_3'	Confining pressure
Fr	Cyclic loading frequency
F_E	Squared error function
E	Young's modulus
γ	Dry unit weight
$\varepsilon_{a,rec}$	Resilient axial strain
FIS	Fuzzy inference system
GUI	Graphical user interface
I	Number of input parameter
M_R	Resilient modulus
$q_{max,cyc}$	Magnitude of cyclic load
MAE	Mean absolute error
MF	Membership function
MC	Moisture content
ML	Machine learning
MLP	Multilayer perceptron
MI	Mutual information
N	Number of cycles
PI	Plasticity index
P#200	Percent passing number 200 sieve
q_{min}	Minimum deviator stress
q_{max}	Maximum deviator stress
RMSE	Root mean squared error
R^2	Coefficient of determination
SVM	Support vector machine
Trimf	Triangular MF
w	Water content
VAF	Variance account for

1. Introduction

As the population of Australia continues to grow, more urban infrastructure is needed to ensure a more efficient plan for public transport in the future; in fact, in many countries and megacities, urban railway construction is considered to be a priority. The layers of granular material on a railway track are formed by an upper layer of ballast that consists of angular particles (i.e., 13–

60 mm in size) and a lower sub-ballast or capping layer that consists of compacted granular material that resembles a broadly-graded road base. When a ballast layer is installed, one of its key functions is to serve as a primary load-bearing layer and to transfer stress on the underlying weaker subgrade to minimise track settlement and ensure rapid drainage [1,2]. The mechanical behaviour of ballast layer under various loading magnitudes and frequencies has been investigated. When considering the elastic response of ballast under cyclic loading, the resilient modulus (M_R) can be defined by the following equation [3]:

$$M_R = \frac{\Delta q}{\varepsilon_{a,rec}} \tag{1}$$

where Δq is the difference between the maximum deviator stress (q_{max}) and the minimum deviator stress (q_{min}), and $\varepsilon_{a,rec}$ is the resilient axial strain (Fig. 1). Even though calculating M_R is similar to computing the secant Young's modulus (E), the latter is commonly used to define the elastic response of the material under monotonic loading. In transportation geomechanics, the resilient modulus, M_R is one of the key design parameters that relates track deformation (vertical strain) to the applied cyclic train loading over a sufficient number of loading cycles (Fig. 1).

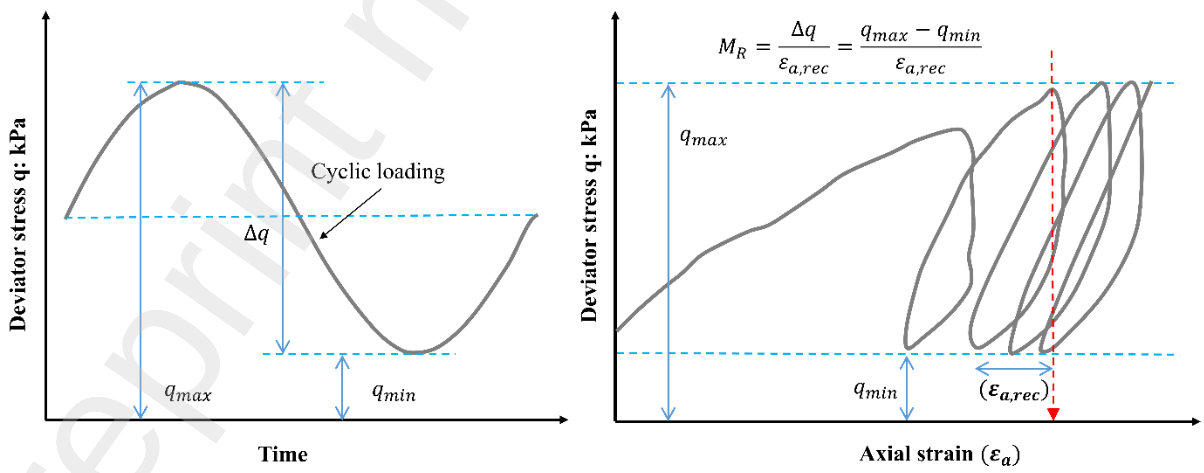

(a)

(b)

Fig. 1. Definition of Resilient Modulus, M_R, (a): the minimum and maximum deviator stresses in cyclic loading curve, (b): axial strain changes during application of one cycle of load

M_R is normally determined by conducting cyclic triaxial tests in the laboratory. Direct tests of determining the M_R have proven to be too expensive in both time and money [4]. Moreover, the large-scale cyclic test for ballast can be complex to operate, requires sample preparation, technical effort, and subsequent analysis before M_R can be measured [5,6]. Therefore, it is better to propose predictive techniques for estimating M_R that are easier and more applicable.

Previous studies into the M_R of soil can be categorised into three major groups, namely (i) experimental/numerical; (ii) statistical; and (iii) artificial intelligence (AI). Experimental/numerical studies focus on evaluating or simulating M_R with properties such as the type of soil, the degree of saturation [7–10], or other relevant parameters such as shear strain, confining pressure, deviator stress, damping ratio, bulk stress, and number of load cycles [11–17]. However, these proposed experimental/numerical solutions still need extensive testing or modelling procedures, all of which require a significant amount of time, expertise and equipment. The second group of models developed for predicting M_R are statistical using regression-based models. The first study carried out by Carmichael and Stuart [18] has proposed two formulae for predicting the M_R of cohesive and granular soils. These formulae are mainly based on different types of soils (CH, ML, GW, and GC), their stress values (deviator and bulk stresses), and properties such as the plasticity index, PI, and water content, w. In another study by Drumm et al. [19], the M_R of subgrade soil is predicted using strength parameters such as the unconfined compressive strength, and elastic modulus, E, and properties such as the percentage of clay, C, PI and dry unit weight, γ. The model showed a good level of accuracy, with the coefficient of determination (R^2) ranging from 0.81-0.83. Khasawneh and Al-jamal [20] introduced linear and non-linear multiple regression equations to estimate the M_R of fine-grained soils; this included using basic soil index parameters (e.g., Atterberg limits and the percent passing number 200 sieve, P#200) and stress-based factors. It seems that the independent variables used to develop statistical equations are likely to be correlated (e.g., Atterberg limits, γ, and others), and therefore, the model is very complex [4]. In fact, several researchers [21] reported that these models are not always robust enough to accurately describe non-linear and complex systems.

The last group of models and suggested solutions for predicting the M_R of soil is AI. These approaches are very effective at discovering complicated correlations between multi-dimensional data that is why many geotechnical researchers have adopted them in the past [22–26]. Moreover, they are fast, dependable, and efficient at recognising patterns and finding the best way to reach the system output [4]. By considering the routine properties of subgrade soil, such as PI, the moisture content (MC), as well as stress conditions such as the confining pressure, Zaman et al. [27] developed different artificial neural network (ANN) models like the multilayer perceptron (MLP) network to predict M_R. They concluded that these models are generally good enough to be used in practice. In another similar study, tree ensemble machine learning (ML) models were used by Pahno et al. [28] to estimate M_R. In these models, they adopted the database published by Kim [29] to implement the model having 17 input parameters, from which they obtained a range of $R^2 = 0.85$-0.95. Heidarabadizadeh et al. [16] also carried out research in this area by using the data available in the literature [4] and a series of support vector machine (SVM) models to improve their results. The results from their SVM models were more accurate than the original study which used the ANN technique [4]. In summary, the predictions for M_R utilising AI techniques were much more accurate than the other groups mentioned. Overall, an R^2 of more than 0.85 was obtained for these studies, which is much better than the empirical/numerical and statistical techniques. It is also important to note that the AI techniques have been suggested as the most accurate models in previous studies related to geotechnical issues [30–32].

It is found that most of the relevant studies are applicable for road/highway and pavement engineering, and furthermore, most of the published methodologies and predictive models for evaluating M_R are related to soft soil and fine-grained materials and also unbound granular materials. To the authors' knowledge, there have been a few M_R studies (e.g., [33,34]) carried out using AI methods on ballast that are relevant to railway applications. In this study, the M_R values of ballast will be predicted using two AI techniques, ANN and the adaptive neuro-fuzzy inference system (ANFIS). Measured values of M_R from the laboratory were used to calibrate and further validate the predicted models. The most effective factors influencing the M_R of ballast material will be considered as predictors, and the results of predictive models will be discussed in detail.

2. Methods and material

2.1 Artificial neural network (ANN) background

With no previous assumptions or mathematical correlations, ANN can be used to represent complex non-linear interactions among parameters. The structure, function, and computation of a biological neural network inspired the creation of ANN are achieved by utilising a large number of operational non-linear computational units [35]. ANNs can be viewed as massively parallel systems in which a network of connected processing units, known as neurons or nodes, is organised into layers. Moreover, the way a network functions and the kind of network it is depends on how its neural connections are configured [36].

The output layer node error is minimised by constantly adjusting the design and connecting weights during network training. In reality, a squared error function (F_E) computes the output error as follows:

$$F_E = \frac{1}{2}\sum_{i=1}^{P}\left(t^{(i)} - y^{(i)}\right)^2 \quad (2)$$

where the actual and predicted values are presented by y and t, respectively. In addition, the parameter P indicates the number of training patterns to be used.

Back-propagation (BP) is a gradient-based learning method that is especially beneficial for multilayer feed-forward networks in the process of network learning [37]. BP learning uses a two-stage approach that incorporates a forward and a backward step as its foundation for each training phase. In this step, input signals are pushed forwards through the network and then each node on the output layer produces an error signal. In the next step, the weights and biases in the network will be changed by sending the error rates backwards through the network.

As a kind of multilayer feed-forward network, MLPs use weighted connections and activation functions between successive layers of processing units (neurons) to communicate and process information (signals) to achieve high performance [35]. Neuron outputs may be generated by the activation functions of hidden and output neurons, which may perform specifically defined activation functions of net input. When a hidden neuron is trained, it receives the complete net input, which is multiplied by an adaptive weight coefficient (w_{ij}) for each incoming signal (x_i) from the previous layer. As a final step, weighted signals are added together, and a small amount of bias is introduced into the resulting total signal. This process is then repeated for all of the layers in the system until the system's complete output is generated. A hidden or output neuron's entire net input may be expressed as follows:

$$net_j = \sum_{i=1}^{n} w_{ij} x_i + b_j \tag{3}$$

where net_j is the network constructed for neuron j, and b_j is the bias of neuron j. The activation function squeezes the whole net input from each neuron's output into a single value (e.g., sigmoid). For each hidden or output neuron, the output can be presented as follows:

The entire net input for each neuron is reduced to the activation function for that neuron (e.g., sigmoid). For each hidden neuron, the output is obtained as:

$$O_j = \frac{1}{(1 + exp\{-net_j\})} \tag{4}$$

Fig. 2 shows a simplified representation of the data-processing procedures of an artificial neuron.

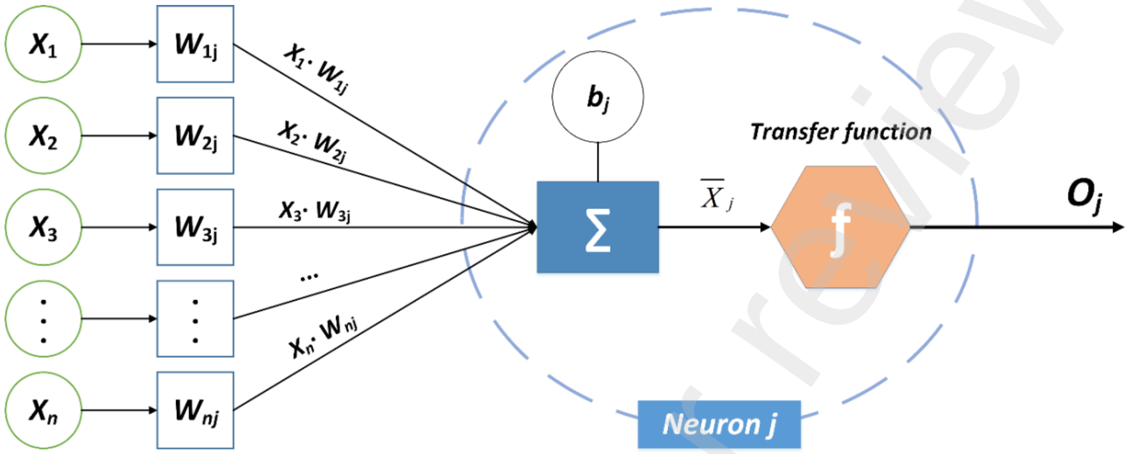

Fig. 2. An artificial neuron *j* with its various components

2.2 Adaptive neuro-fuzzy inference system (ANFIS) background

Jang [38] was the first to introduce the ANFIS technique, a functional mapping concept that approximates the process of predicting the values of internal system parameters that can be simulated using ANFIS capabilities. The notion of fuzzy inference or rule-based systems is included in ANN, which is why this AI approach is referred to as neuro-fuzzy. The primary goal of ANFIS is to map a connection between the parameters that are system input and those that are system output by defining a series of membership functions (MFs) for the variables. The ANFIS network structure is divided into two sections: the premise and the consequence. The training part of ANFIS is the process of tuning the parameters of these sections using an algorithm. During training, ANFIS employs the existing input–output data pairings, after which IF-THEN fuzzy rules that indicate the interconnection of these components are generated [38,39]. Fig. 3 shows the five-layer structure of ANFIS where a two-input (x_1, x_2), and one-output ANFIS structure with three rules are shown. A breakdown of the layers of ANFIS, based on the diagram shown in Fig. 3 is presented in the following five layers:

The first layer: fuzzification

Fuzzy clusters are generated from input data in the fuzzification layer. The structure of the underlying data MFs are used in the fuzzification layer. These are called "premise parameters" and they define the structure of the MFs. Equations 5 and 6 are used to compute the membership degrees of each MF, where $\{h,j,k\}$ is the set of premise parameters. In this layer, the membership degrees gained are represented by $\mu_{x_1}$and μ_{x_2}. The $gbellmf$ is defined as Guassian MF in these equations.

$$\mu_{A_i}(x) = gbellmf\ (x; h,j,k) = \frac{1}{1 + \left|\frac{x-k}{h}\right|^{2j}} \tag{5}$$

$$Y_i^1 = \mu_{A_i}(x) \tag{6}$$

The second layer: *Rule*

The membership values of the fuzzification layer (the first layer) are used to create firing strengths (w_i) for rules. The membership values are multiplied to get the w_i values, as presented in Equation 7.

$$Y_i^2 = w_i = \mu_{A_i}(x_1).\mu_{B_i}(x_2) \qquad i=1,2 \tag{7}$$

The third layer: Normalization

For each rule, the normalisation layer estimates the average firing strength for that specific rule. Using the normalised value, the ratio of the i^{th} rule's firing strength to the sum of all firing strengths is calculated (Equation 8).

$$Y_i^3 = \overline{w_i} = \frac{w_i}{w_1 + w_2 + w_3 + w_4} \qquad i \in \{1, 2, 3, 4\} \tag{8}$$

The fourth layer: Defuzzification

The values of the rules are computed in each node of this layer (defuzzification) using the weighted values provided above, as given in Equation 9. A first-order polynomial is used to calculate this number.

$$Y_i^4 = \overline{w_i} f_i = \overline{w_i} \left(r_i x_1 + s_i x_2 + t_i \right) \tag{9}$$

where $\overline{w_i}$ is obtained as the output of the previous layer, and r_i, s_i, and t_i are the parameter set (also known as the consequence parameters) which will be used to calculate the system output Y. The number of consequence parameters is considered as $m + 1$ where m is the number of input variables.

The fifth layer: Summation

The final result of ANFIS in this layer will be found by adding up the results that each rule in the defuzzification layer produces (Equation 10).

$$Y_i^5 = \text{overalloutput} = \sum_i \overline{w_i} f_i = \frac{\sum_i w_i f_i}{\sum_i w_i} \tag{10}$$

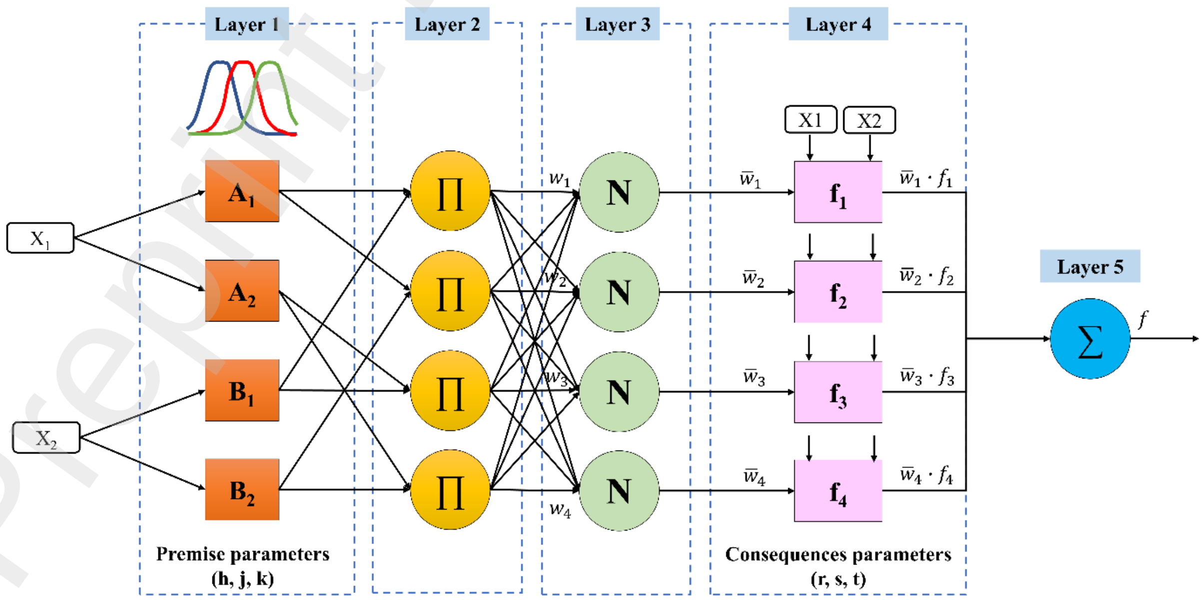

Fig. 3. The schematic view of the five-layer architecture of ANFIS

2.3 Established database

Previous studies related to the determination and prediction of M_R have been reviewed and found that for the same ballast material and source, there are still some parameters that can affect the M_R. Sun et al. [5,6,40], Navaratnarajah and Indraratna [41] and Thakur et al. [42] studied the effects of the cyclic loading frequency (Fr) and the number of cycles (N) on ballast deformation and reported that these two parameters play a significant role. On the other hand, stress related parameters such as the magnitude of cyclic load ($q_{max,cyc}$), the confining pressure (σ_3'), and the deviator stress are considered to be the most influential factors that affect the final results of ballast deformation [1,42–44]. So, it is essential that such parameters will be selected as input parameters to predict ballast M_R in this study. Since there is a need to have an acceptable variation for each effective parameter in AI studies, some parameters such as compacted density of ballast and other physical properties are not considered as input parameters in the current analysis. Therefore, four parameters ($q_{max,cyc}$, σ_3', Fr, and N) are used as model inputs or predictors; hence the M_R can be predicted by a function of $M_R = f\,(q_{max,cyc}$, σ_3', Fr, and N).

In order to fulfil the aims of this study, the study and tests carried out by Sun et al. [6] were considered. The volcanic latite basalt utilised by Sun et al. [6] is a common ballast that is extracted from quarries and then used in railway projects in New South Wales, Australia. These specimens are produced in accordance with the relevant Australian standards [45], and after being sieved, rinsed, and mixed together, they are then compacted in three distinct layers inside a rubber membrane. Afterwards, a series of drained triaxial tests under different cyclic conditions were carried out on the specimens using a large-scale triaxial apparatus. These tests are based on different values for each predictor used in this study ($q_{max,cyc}$, $\sigma_3^{'}$, Fr, and N) and their M_R values are recorded. Eventually, a database with 219 data samples was prepared such that each data sample contains four inputs and one output.

In this database, outliers were identified beforehand and the data was cleaned. One data point that stands out from the rest is called an outlier. An outlier could be due to variations in the measurement, or experimental inaccuracies; in each case the results of the experiment should be omitted from the database. This process enabled 23 outliers which were identified in the database through the method of identifying outliers. The outliers are then removed from the database, leaving 196 data samples to be considered for modelling in this study. Some basic information about the selected database can be seen in Table 1. Further details regarding the tests and their conditions can be found in the original study [6].

To better understand the data, histograms of all the input and output parameters are shown in Fig. 4, and 'violin plots' of the same parameters are shown in Fig. 5. Numerical data that is plotted as a violin plot may be thought of as a mixture of a box plot and a Kernel density plot [46]. The median (a red point on the violin plot) and inter-quartile range (the black bar in the middle of the violin) can be discovered in the violin plots, which can effectively display the complete distribution of data. The data distribution of these variables is heterogeneous, and is usually concentrated around one or several values. The modelling procedure for predicting the M_R will be presented in the following sections.

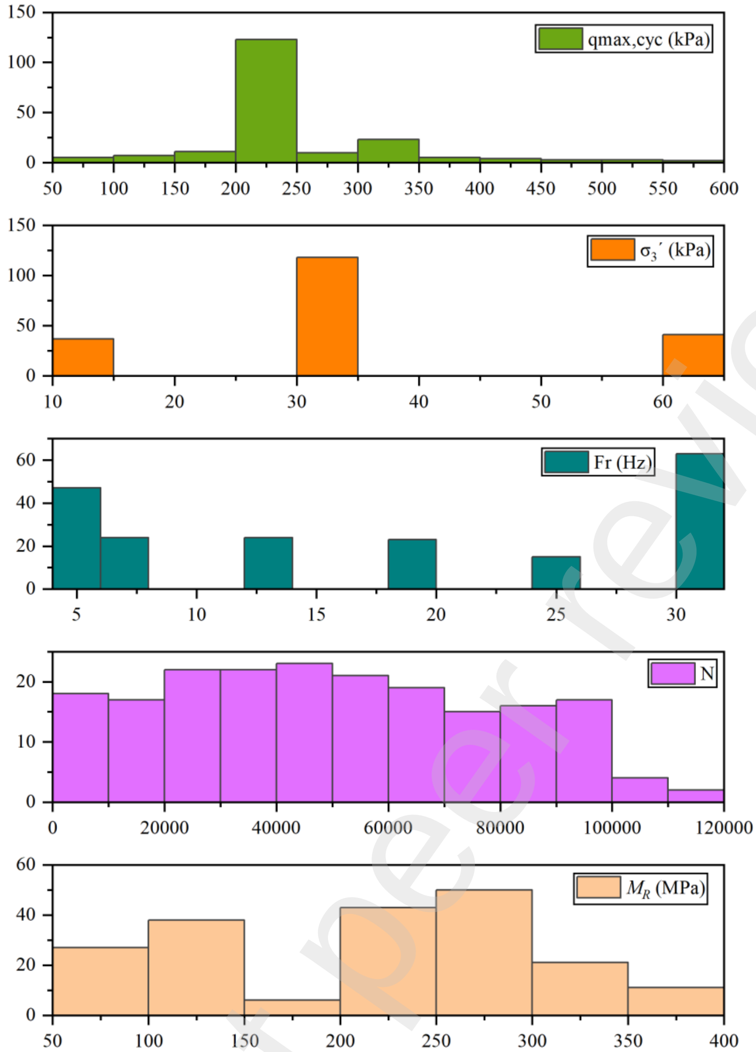

Fig. 4. Histograms for different variables used in this research

Table 1. Statistical information regarding variables used in this research to predict ballast M_R

Variable	**Category**	**Symbol**	**Min**	**Max**	**Ave**
Magnitude of cyclic load (kPa)	Input	$q_{max,cyc}$	87.5	555	250.5
Confining pressure (kPa)	Input	σ_3'	10	60	32.5
Cyclic loading frequency (Hz)	Input	Fr	5	30	17
Number of cycles	Input	N	254	112527	49263
Resilient modulus (MPa)	Output	M_R	67.6	384.9	215.4

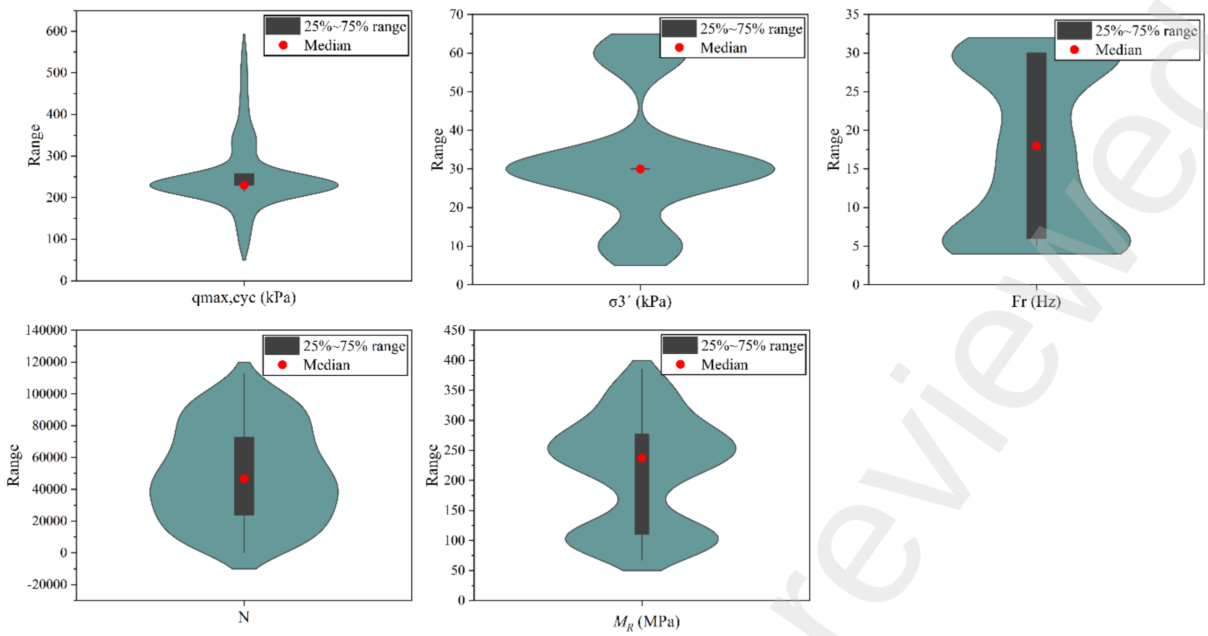

Fig. 5. Violin plot for each parameter used in this research

2.4 Evaluation indices

To evaluate the accuracy and robustness of the predictive models in this study, five evaluation metrics, i.e., R^2, the variance account for (VAF), the root mean squared error (RMSE), A-20 index, and the mean absolute error (MAE) are considered. R^2 is the square of the correlation between the values that are predicted and those that are actually measured. The value of the VAF (per cent) indicates how well the prediction is made by comparing the standard deviation of the fitting error to the standard deviation of the actual value. These evaluation metrics can be found in Equations 11-15. The root mean squared error (RMSE) represents the standard deviation of the fitting error that occurs between the predicted value and the measured values, while the mean absolute error (MAE) represents the value that is most likely to occur when the actual values are compared to the estimated values. In addition, the A-20 index shows that the ratio of the results in each stage is within 0.8-1.2 times the measured or actual data samples. The formulae for these evaluation indices are presented as follows:

$$R^2 = 1 - \frac{\sum_{i=1}^{N}(M_{Rmea} - M_{Rpre})^2}{\sum_{i=1}^{N}(\tau_{mea} - \overline{\tau_{mea}})^2} \qquad (11)$$

$$VAF = \left(1 - \frac{var(M_{Rmea} - M_{Rpre})}{var(M_{Rmea})}\right) \times 100\% \tag{12}$$

$$RMSE = \sqrt{\frac{1}{D}\sum_{i=1}^{D}(M_{Rmea} - M_{Rpre})^2} \tag{13}$$

$$MAE = \frac{1}{D}\sum_{i=1}^{D}|M_{Rmea} - M_{Rpre}| \tag{14}$$

$$A-20 = \frac{m20}{D} \tag{15}$$

where M_{Rmea}, M_{Rpre}, $\overline{M_{Rmea}}$ denotes the measured, predicted, and mean value of the M_R, respectively. $m20$ is the number of samples for which the predicted M_R values that are in the range of 0.8~1.2 times the actual M_R values; D is the total number of data samples. It is noted that when the predicted values and the measured values of M_R are precisely the same, R^2 is 1, the VAF is 100%, the RMSE is 0, A-20 is 1, and the MAE is 0.

3. Modelling process

This section discusses the methods and modelling steps used to predict M_R values where two predictive techniques, ANN, and ANFIS are adopted.. The process for modelling these non-linear approaches will be discussed in this section, while their accuracy to predict the M_R of ballast will be evaluated later.

3.1 ANN

The first stage of modelling is to randomly divide the entire database into training, testing, and validation portions. The samples of training data are to train a large portion of the data to discover and learn possible patterns, whereas the testing data samples should be used to assess the level of accuracy of the trained model. A small portion of the total data samples are used for validation to ensure that the developed model has been generalised enough and that it can be optimised. While a single percentage of 20, 25, and a range of 20-30 are recommended in the literature as testing data samples [47,48], some researchers used up to 70% of the whole data samples as training sets and solved their problems perfectly [49]. With validation, researchers targeted a range of 10-15% to check model generalisation [50]. In this study, a combination of 70, 20, and 10% of the whole database (i.e., 196) is selected as training, testing, and validation parts, respectively. It is noted that the data samples for training, testing, and validation are selected randomly from the entire database where each sample has the same probability of being chosen as other samples.

The ANN modelling process should be started by normalising the whole database (i.e., training, testing and validation) in a limited range [0-1]. This is carried out for each input/output parameter using $L_{norm} = (L - L_{min})/(L_{max} - L_{min})$, where L_{max} and L_{min}, are the maximum and minimum values of parameter L, respectively, and L_{norm} is the normalised form of parameter, L. The number of hidden layers and the node(s) inside each hidden layer are considered to be the two most important factors in obtaining an accurate MLP predictive model. Hornik et al. [51] showed that when there are a sufficient number of hidden nodes, any complicated fitting problem may be approximated by a single hidden layer in the modelling of MLP. One hidden layer with a sigmoidal activation function is used for each MLP network, and one output layer (M_R) is used for each network.

If there are any hidden node numbers, some formulae have been suggested by various scholars, most of which depend on the number of input variables, I, (e.g., $2I/3$, $2I$) [52,53]. Therefore, a sufficient range and number of hidden nodes should be designed. The upper bound for the hidden node number recommended by Hecht-Nielsen [54] was $2I + 1$. Taking into account all the available formulae for determining hidden node numbers, as well as the number of input parameters in this study (I = 4), a range of 1–9 has been implemented in a trial-and-error process. Nine MLP models were constructed and the results were assessed using the R^2 values as reported in Table 2. It is seen that the hidden node number has a significant effect on the system's performance because by increasing the hidden node number from 1-5, the model will become more accurate. However, it seems that selecting the most accurate MLP model may be complicated because some R^2 results are very similar; and to overcome this, a simple ranking method introduced by Zorlu et al. [55] was applied to select the most accurate MLP model. A higher score on the training set represents the greatest learning capacity, and a greater capability on the testing and validation sets means the model has the ability to generalise and can be applied practically. Therefore, the highest R^2 (e.g., 0.966 for the training set) received a rank of 9, followed by lower ranks for the other R^2 values. If different MLP models have the same value for R^2, their rank will be the same as those models. The total ranking would eventually be a summation of rankings for the training, testing, and validation parts of each MLP model. According to the total ranking values, model number 8, with a rank of 25, represents the highest performance prediction in forecasting M_R. The R^2 values of this MLP model are 0.966, 0.928, and 0.942, respectively, for training, testing, and validation. These results showed that MLP is capable to map M_R behaviour by considering the effects of four input parameters (i.e., $q_{max,cyc}$, σ_3', Fr, and N). Note that the normalised measured and predicted M_R values have been normalised again to calculate other performance prediction indices. The results and capability of the ANN model will be discussed further in the "Results and Discussion" section.

Table 2. Nine built MLPs to predict ballast M_R

Hidden Node Number	R^2			Ranking			Total Ranking
	Training	Testing	Validation	Training	Testing	Validation	
1	0.762	0.706	0.830	3	1	1	5
2	0.865	0.824	0.872	4	3	2	9
3	0.918	0.870	0.933	5	4	4	13
4	0.931	0.912	0.931	6	5	3	14
5	0.966	0.925	0.939	9	7	6	22
6	0.949	0.918	0.935	7	6	5	18
7	0.966	0.817	0.968	9	2	9	20
8	0.966	0.928	0.942	9	9	7	25
9	0.956	0.925	0.964	8	8	8	24

3.2 ANFIS

This section explains the detailed ANFIS modelling for predicting the M_R values in the form of a combination of four input parameters (i.e., $q_{max,cyc}$, σ_3', Fr, and N). Modelling and regulating non-specific and uncertain systems may be accomplished with the help of ANFIS, an intelligent neuro-fuzzy technique. The implementation of ANFIS is commonly carried out in the following processes. Firstly, after selecting the predictors and the output of the network, the type and number of MF should be determined. Then, fuzzy rules to solve the particular problem should be established.

The suggested ANFIS structure must be trained, tested, and validated, so an instrument must be built for that purpose in a MatLab software environment. It is possible to construct a variety of ANFIS models with various parameters by using the graphical user interface (GUI). This application provides users with a fuzzy inference system (FIS) editor, a rule editor, an output surface viewer, an MF editor, and a fuzzy inference viewer; this programme also includes an output surface viewer. The GUI selection panel of the ANFIS editor is responsible for the beginning of FIS training, testing, and validation, the saving of the FIS object, and the presentation of the fuzzy rules and MFs.

Previous studies have emphasised the effectiveness of MF design using the Gaussian MF (Gaussianmf) because it offers simplicity and flexibility [56], but the performance of the ANFIS models was suitable enough when other types of MF such as Triangular MF (Trimf) are used [57]. On the other hand, the number of MF for each input plays a significant role on the system's performance. Therefore, the six ANFIS models reported in Table 3 were created and their corresponding results regarding training, testing, and validation were obtained. The values of 3, 4, and 5 were applied to the number of MFs for each type of MF (i.e., Trimf and Gaussianmf). In these models, the linear output MF type is utilised for the output (M_R). It is found that the models became more accurate when the number of MFs for each input were increased. Note that the number of fuzzy rules will increase if the number of MFs for each input is increased. For example, considering the number of inputs in this study (i.e., 4), the total number of fuzzy rules for MF = 3 and MF = 5 is $3^4 = 81$ and $5^4 = 625$, respectively. Therefore, to keep the number of fuzzy rules as reasonable as possible, the authors used 3, 4 and 5 as the number of MFs for each input parameter. The results obtained are quite similar (Table 3), so the same ranking system in the ANN part was applied. The best total rank, which is based on R^2 and RMSE for training, testing, and validation stages, is 33. So, the ANFIS model number 3 with Trimf as the MF type and 5 MFs in each input was selected as the best ANFIS model for predicting ballast M_R.

The MFs designed by the best ANFIS model to estimate ballast M_R are shown in Fig. 6. The range of input parameters used in the training phase are divided into five parts, namely very low (VL), low (L), medium (M), high (H), and very high (VH). In addition, some of the If-Then rules created by the system when predicting ballast M_R are shown in Table 4. The ANFIS models are trained using the linguistic variables and the If-Then rules to predict ballast M_R. The same variables and rules are used to test and validate the trained model. In the next section, the results from the best ANFIS model will be examined in more depth.

Table 3. Six ANFIS models with different specifications and their predictive performance

ANFIS model	MF type	No. of MF in each input	Network Performance						Ranking						Total Ranking
			R^2 train	R^2 test	R^2 validation	RMSE train	RMSE test	RMSE validation	R^2 train	R^2 test	R^2 validation	RMSE train	RMSE test	RMSE validation	
1	Trimf	3	0.952	0.813	0.883	18.95	40.455	32.864	4	3	4	3	3	3	20
2	Trimf	4	0.966	0.894	0.912	15.993	30.059	28.619	5	6	5	4	6	4	30
3	Trimf	5	0.970	0.874	0.922	15.11	32.696	27.387	6	5	6	5	5	6	33
4	Gaussianmf	3	0.926	0.744	0.853	23.554	46.83	36.942	3	2	3	2	2	2	14
5	Gaussianmf	4	0.966	0.894	0.912	15.993	30.059	28.619	5	6	5	4	6	4	30
6	Gaussianmf	5	0.970	0.863	0.922	14.962	34.272	28.146	6	4	6	6	4	5	31

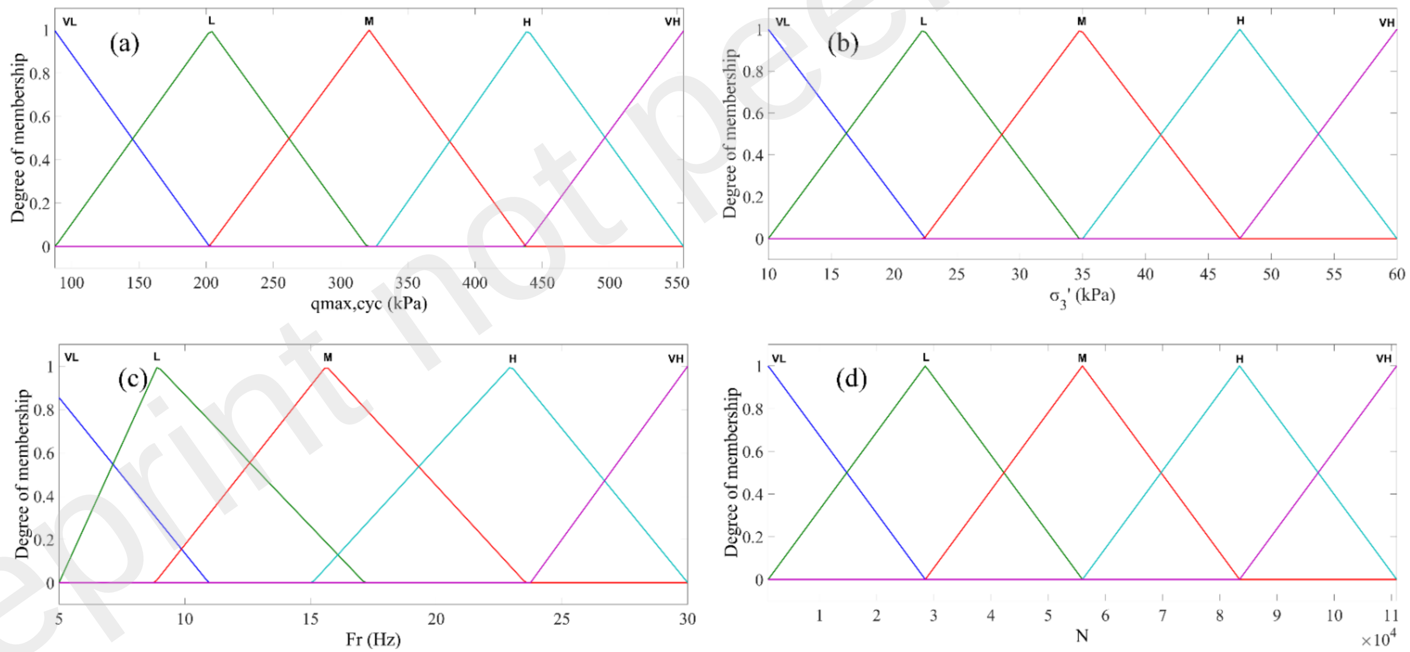

Figure 6. MFs used in this study by the ANFIS model, (a) $q_{max,cyc}$, (b) $\sigma_3^{'}$, (c) Fr, and (d) N

Table 4. Some examples of the If-Then ANFIS rules used to predict M_R

If ($q_{max,cyc}$ is VL) and (σ_3' is VL) and (Fr is VL) and (N is VH) Then (M_R is VL)
If ($q_{max,cyc}$ is L) and (σ_3' is L) and (Fr is L) and (N is VH) Then (M_R is L)
If ($q_{max,cyc}$ is M) and (σ_3' is M) and (Fr is L) and (N is VH) Then (M_R is M)
If ($q_{max,cyc}$ is H) and (σ_3' is VH) and (Fr is M) and (N is L) Then (M_R is H)
If ($q_{max,cyc}$ is VH) and (σ_3' is H) and (Fr is VH) and (N is VH) Then (M_R is VH)

4. Results and discussion

4.1 Model assessment

The predictive models should be evaluated in the training phase, and in the case of satisfaction, they should also be evaluated in the testing and validation stages. The best model is the one that receives an acceptable level of predictions for all phases. In this study, the calculated performance indices (Equations 11-15) for the training, testing, and validation of the non-linear predictive models are shown in Table 5. In terms of system error, the RMSE values of (32.696 and 25.122) and (27.387 and 22.778) and the MAE values of (21.292 and 18.174) and (18.404 and 17.106) are obtained for the testing and validation phases of the ANFIS, and ANN models, respectively. With ANN and ANFIS, the results are similar, although the ANFIS predictions during the training phase are better, and the testing and validation phases reported closer measured and predicted M_R values by the ANN model. A-20 is a good index to identify the best models because it calculates the predicted over measured M_R values within a certain range (0.8-1.2). The results of A-20 show that ANN is a more accurate AI technique than ANFIS with regards to training, testing, and validation.

In order to have a better understanding, the measured M_R vs predicted M_R for all phases of the ANN and ANFIS models are shown in Figs. 7 and 8, respectively. These figures confirm that the ANFIS and ANN models are capable to predict M_R values that are close to the measured ones. The Taylor diagrams of the training, testing and validation outcomes are shown in Fig. 9. The distance that separates the point that represents the model and the point of origin is used to illustrate the standard deviation, and the ticks that appear on the arc that revolves clockwise around the point that represents the model, are used to illustrate the correlation coefficient. The actual M_R value is represented by the point labelled "REF" (the black star), and the distance from each of the other points to the point labelled "REF" reflects the centred system error. When working with Taylor diagrams, the placement of points on the graph may be used as a criterion for determining the capabilities of the relevant model. The models that are represented by points located closer to the "REF" point are more capable, so according to this guiding concept, the ANFIS model performed best in the training phase, whereas the ANN model was more accurate during the testing and validation phases. Although the ANN and ANFIS models were very accurate, a secondary validation may be needed to examine the accuracy of the ANN and ANFIS models built in this study. To do this, the authors used a new database from literature; it will be explained in the following section.

Table 5. The results of M_R obtained for the training, testing and validation phases

Model	Training					Testing					Validation				
	R^2	VAF (%)	RMSE	A-20	MAE	R^2	VAF (%)	RMSE	A-20	MAE	R^2	VAF (%)	RMSE	A-20	MAE
ANFIS	0.970	96.970	15.110	0.971	10.412	0.874	87.405	32.696	0.872	21.292	0.922	92.072	27.387	0.900	18.404
ANN	0.966	96.619	15.965	0.978	11.316	0.928	96.625	25.122	0.949	18.174	0.942	94.125	22.778	0.950	17.106

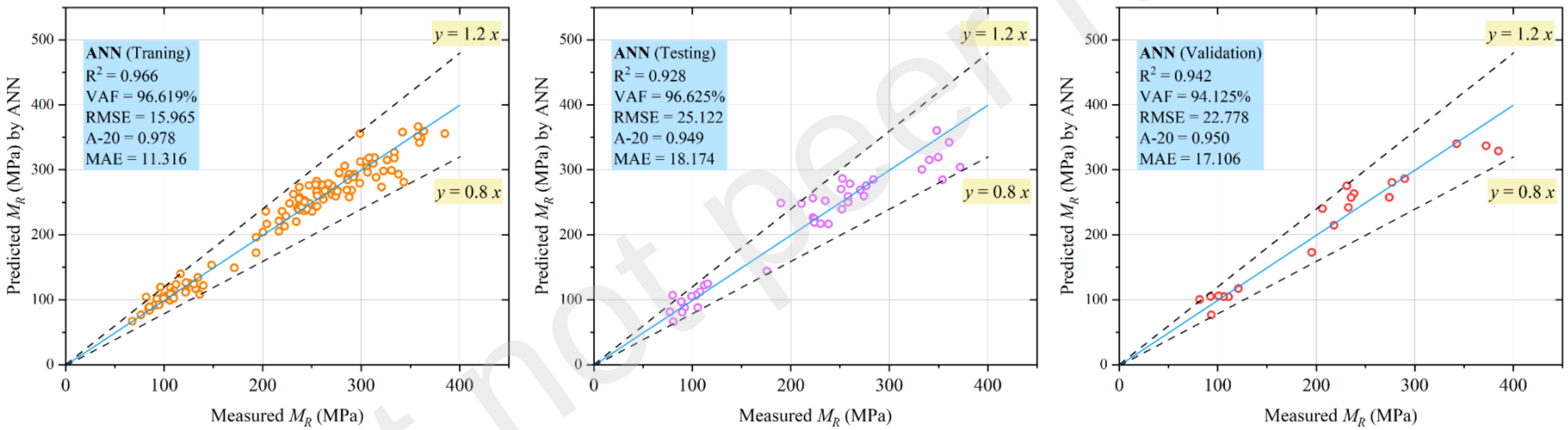

Fig. 7. Measured M_R vs predicted M_R in the case of ANN model

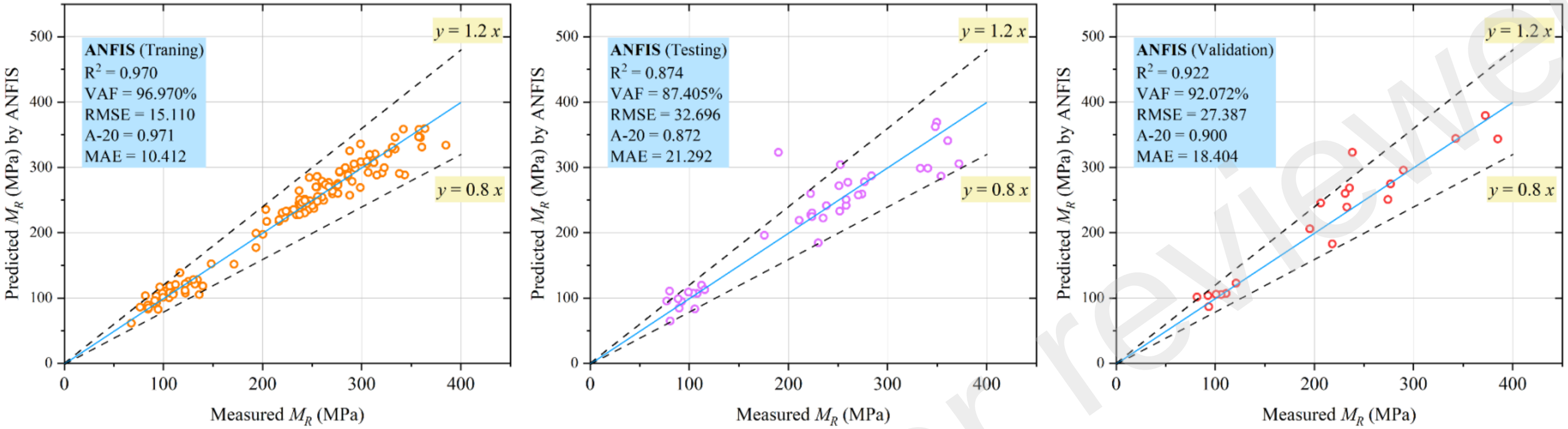

Fig. 8. Measured M_R vs predicted M_R in the case of ANFIS model

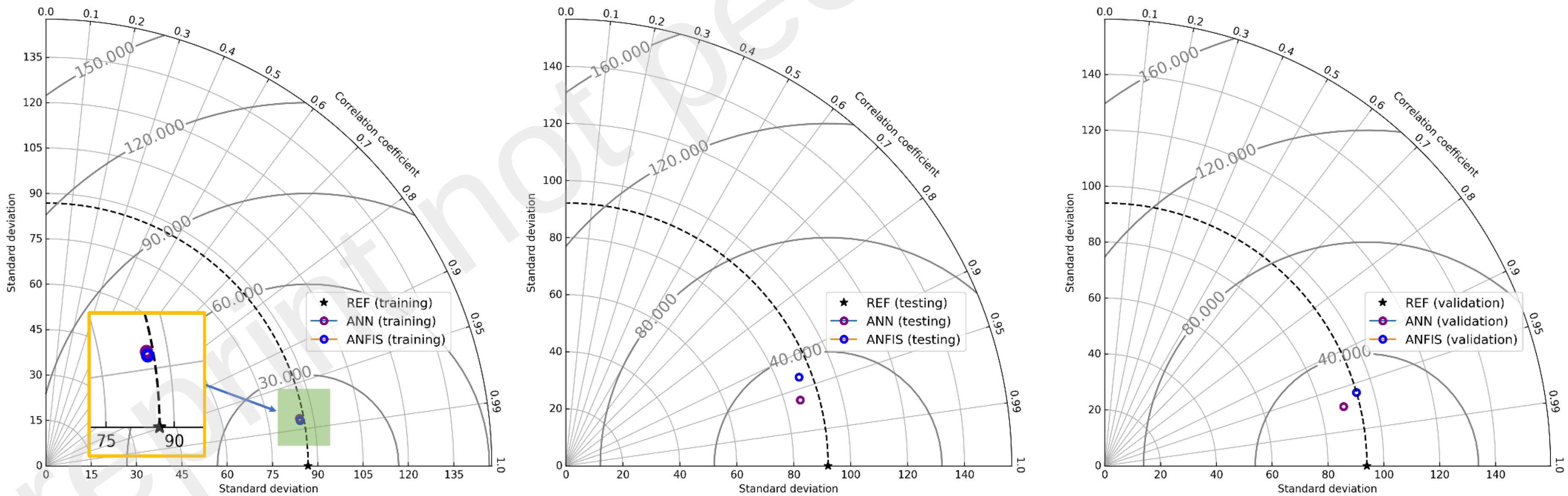

Fig. 9. Taylor diagram for all phases and two predictive models

4.2 Validation with the other studies

This section describes the process of performing a secondary validation phase to determine the best model in this study. In this regard, 37 new independent data samples with the same input parameters were randomly collected from the literature, as presented in Table 6. As shown, some inputs are within the range of inputs used to construct the models. For example, $q_{max,cyc}$ is the same for all 37 data samples (i.e., 230 kPa), and the range for $\sigma_3^{'}$ is between 10-60 kPa. However, some data points are outside the ranges considered while developing the model for this study. The *Fr* range in Table 1 is (5-30 Hz), whereas some points with *Fr* = 40 Hz are in Table 6. In addition, some out-of-range values for *N* (i.e., 200,000, 300,000, and 400,000) compared to Table 1 were considered in these validation data samples. All predictive models, namely ANN, and ANFIS, were applied to the data samples in Table 6 to challenge them when predicting M_R values if new data is available. It is important to note that the source and type of ballast used in Table 6 are the same as the original data samples used in model development.

After conducting the analyses using new data, the results were obtained and then the measured M_R and predicted M_R were compared. The best way to assess the model's performance in this stage is by system error. A large amount of RMSE i.e., 235 was obtained for ANN model, but the system error (i.e., RMSE) for the ANFIS model is 31.2 which was the most accurate of all predictive models. An R^2 of 0.709 was obtained between measured and predicted M_R values using the ANFIS model; this confirms that this model can predict M_R values for training, testing, and primary validation, and for regarding the secondary part of the validation.

As discussed earlier, ANFIS is a combination of the ANN and fuzzy logic controllers, which means the fuzzy rules are generated using ANN. This is one of the key differences between ANN and ANFIS. The controller blocks, and parameters of ANN are generated in accordance with an algorithm, whereas ANFIS is a combination of ANN and fuzzy logic controllers. The incorporation of neural networks into fuzzy systems not only enhances their performance, it also provides a better representation of their internal information thanks to the ability of neural networks to learn [58]. The measured and predicted M_R values during the secondary validation are shown in Fig. 10. It is seen that the ANFIS model can be used as a strong predictive model to estimate ballast M_R for the situation described in this study.

Table 6. The selected data samples for the purpose of secondary validation

$q_{max,cyc}$ (kPa)	$\sigma_3^{'}$ (kPa)	Fr (Hz)	N	M_R (MPa)	Reference
230	30	5	1000	198.1	Sun et al. [40]
230	30	5	2000	218.5	
230	30	5	5000	220.5	
230	30	5	10000	240.8	
230	10	10	1000	215.5	
230	10	10	2000	223.5	
230	10	10	5000	261.5	
230	10	10	10000	305.7	
230	60	5	1000	247.7	
230	60	5	2000	254.9	
230	60	5	5000	314.7	
230	60	5	10000	323.9	
230	60	5	25000	345.5	
230	15	15	50000	186.3	Navaratnarajah and Indraratna [41]
230	15	20	30000	195.1	
230	15	20	50000	196.9	
230	15	20	70000	197.4	
230	20	10	50	103.7	Indraratna et al. [11]
230	20	10	100	121.6	
230	20	10	500	144.2	
230	20	10	1000	146.9	
230	20	10	5000	160.5	
230	20	10	10000	158.2	
230	20	10	50000	168.9	
230	20	10	200000	180.3	
230	20	20	50000	176.1	
230	20	20	100000	186.8	
230	20	20	200000	182.5	
230	20	20	300000	189.3	
230	20	30	200000	198.6	
230	20	30	300000	199.8	
230	20	30	400000	200.7	
230	20	40	500	188.9	
230	20	40	1000	197.7	
230	20	40	5000	208.1	
230	20	40	10000	205.9	
230	20	40	50000	214.5	

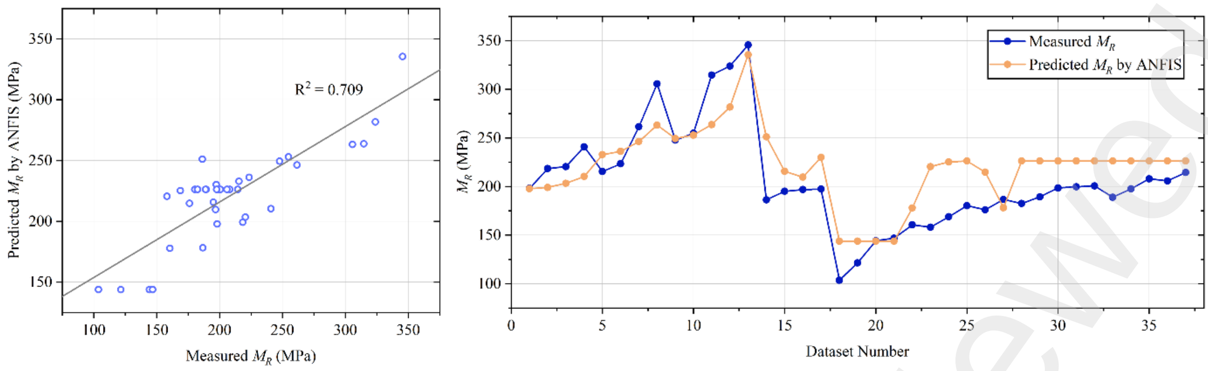

Fig. 10. Predicted M_R values by the ANFIS model vs measured M_R for the secondary validation phase

4.3 Comparison of predicted M_R with previous models

There are several empirical equations that were developed for predicting ballast M_R during the past decades [6,43,59], among others. This section compares the results of ANFIS developed in this study with the empirical equations available in the literature and show that the ANFIS model performs better and more accurately. The bulk stress (∅) is the main parameter in those empirical equations for predicting ballast M_R. There is another study that considered another parameter related to tested frequency for ballast (i.e., *Fr*) [40]. Therefore, the authors decided to select the following empirical equations introduced earlier by Indraratna et al. [43] and Sun et al. [40]. The testing conditions and ballast types of these studies are very similar to the current research.

$$M_R = 40\emptyset^{0.34} \tag{16}$$

$$M_R = a\,.\,F_r^b + \emptyset^c\ (a = 98.6, b = 0.404, c = 0.911) \tag{17}$$

where, ∅ in these equations, is the bulk stress, F_r is the frequency, and *a*, *b* and *c* are constants with specific values. For comparison purposes, the first 25 data samples in Table 6 have been selected and the M_R values were calculated through Equations 16 and 17, accordingly. Fig. 11 shows the measured M_R values in comparison with the predicted M_R values by the ANFIS, and empirical Equations 16 & 17. In addition, Table 7 presents the absolute errors obtained for each data sample as well as the average error (percentage) for each model. It is observed that the ANFIS model is able to predict M_R values closer to the measured values compared to other models. The results of Equation 16 are almost constant with very small changes while we have a wide range for the measured M_R (approximately 100-350 MPa, black line). The results obtained from the Equation 17 deviate far from the measured M_R values from the laboratory tests. One of the possible reason may be related to the role and function type of Fr in this equation. Moreover, the average absolute errors of 13.33, 42.44, and 111.70% obtained for the ANFIS, Equation 16 and Equation 17, respectively (Table 7), confirm that the ANFIS is a more reliable model which is able to estimate M_R values with a high level of accuracy.

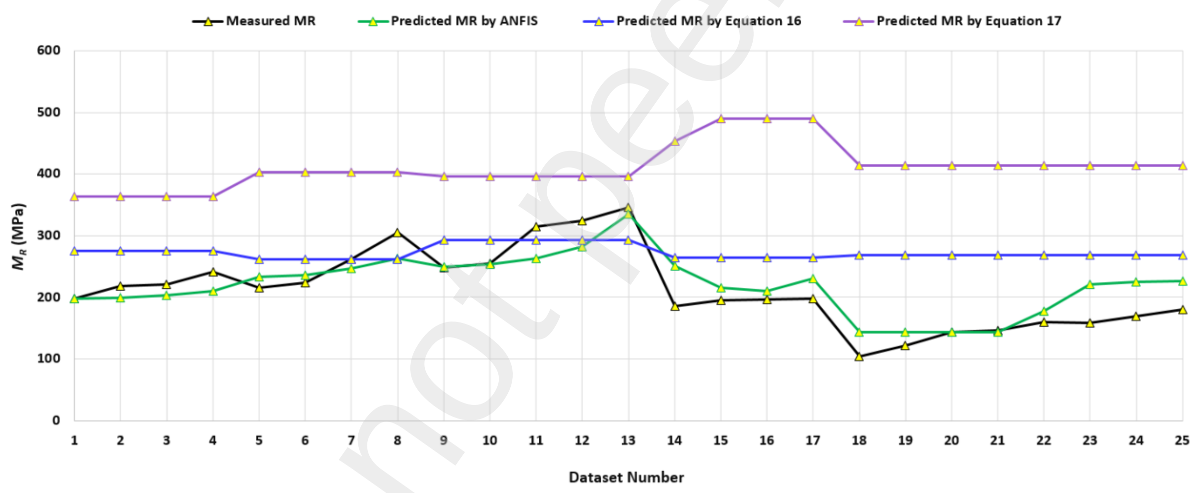

Fig. 11. The measured M_R values in comparison with the predicted M_R values by ANFIS and empirical equations

Table 7. The absolute errors obtained for each data sample as well as the average error for each model

Dataset Number	Absolute Error (%)		
	ANFIS	Equation 16	Equation 17
1	0.17	38.79	83.73
2	8.84	25.87	66.62
3	7.77	24.70	65.08
4	12.64	14.17	51.13
5	8.06	21.34	87.01

6	5.69	17.00	80.31
7	5.79	0.01	54.10
8	13.89	14.47	31.82
9	0.68	18.34	60.16
10	0.75	15.01	55.66
11	16.19	6.85	26.08
12	13.04	9.50	22.48
13	2.89	15.16	14.82
14	34.76	42.20	143.11
15	10.59	35.80	150.77
16	6.50	34.56	148.48
17	16.58	34.22	147.85
18	38.70	158.79	299.24
19	18.30	120.73	240.53
20	0.24	86.14	187.17
21	2.06	82.73	181.90
22	10.83	67.20	157.94
23	39.44	69.65	161.73
24	33.42	58.93	145.19
25	25.52	48.88	129.68
Average	***13.33 %***	***42.44%***	***111.70%***

5. Design considerations

After confirming that the ANFIS model developed in this research is a powerful and applicable predictive technique, it is a further step to extend the database based on this model. To this end, 320 kPa was considered as $q_{max,cyc}$ for the analysis. Then, values of 10 and 20 Hz were considered for Fr. In addition, values of confining pressures (20, 30 and 40 kPa) and loading cycles (10,000, 20,000, 30,000, 40,000 and 50,000 cycles) were used for σ_3' and N, respectively. The idea is to generate a database according to these values and then predict the ballast M_R. In this way, the behaviour of ballast M_R under different conditions can be better investigated and the results can be used by practising engineers. Fig. 12 shows the predicted results of M_R under different loading conditions ($q_{max,cyc}$ = 320 kPa). The predicted curves are in bell-shaped where the M_R values are relatively low in the early cycles (N = 10,000 cycles), followed by gradual increase until reaching the peak at (N = 30,000 cycles), and then decrease in the subsequent loading cycles (N = 50,000 cycles). It seems that the number of loading cycles of N = 30,000 can be introduced as an optimum number. The highest M_R was obtained by the green line when σ_3' is 30 kPa, N is 30,000 cycles and Fr = 20 Hz. Additionally, the lowest M_R

is reported by the red line when σ_3' is 20 kPa, N is 30,000 cycles, and Fr = 20 Hz. Very close values were obtained for two different cases, namely (σ_3' = 40 kPa, and Fr = 10) and (σ_3' = 20 kPa, and Fr = 10), this shows the lesser effects of σ_3' compared to Fr on the model output.

It is also seen that at the beginning (N = 10,000 cycles), in the cases of red, yellow, purple, and black curves, the M_R values are not that close to each other; whereas at the end of the analysis (N = 50,000 cycles), these lines are too close to each other. It shows that by increasing the number of cycles (i.e., N > 30,000), the M_R values are closer for different loading conditions. It is important to note that the results presented in Fig. 12 obtained by simultaneously applying the four parameters, and the results would be different if these parameters were applied separately.

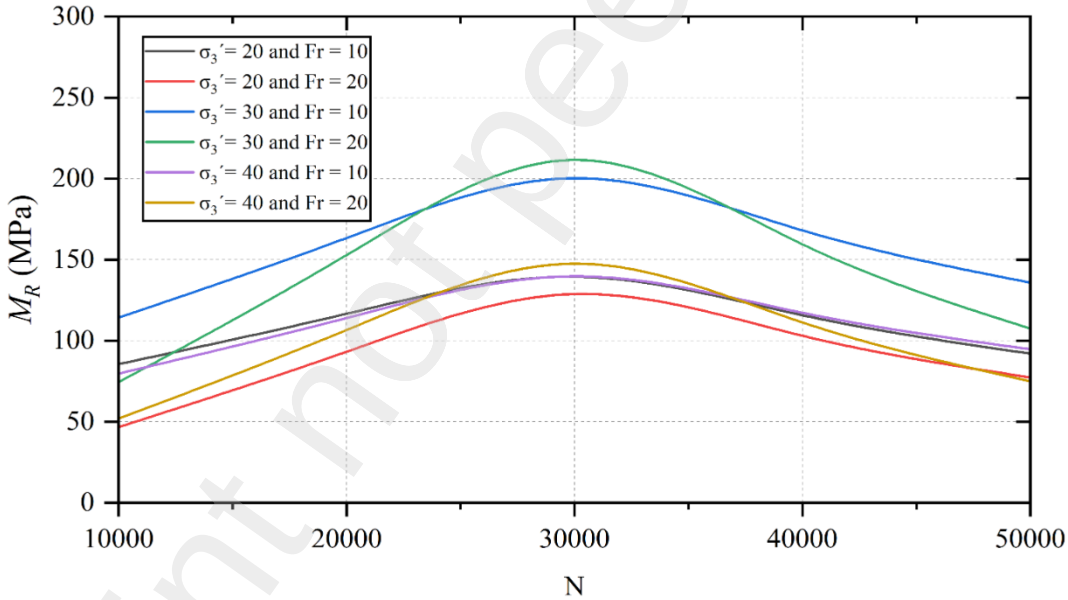

Fig. 12. M_R obtained by the ANFIS model for different N, Fr and σ_3' ($q_{max,cyc}$ = 320 kPa)

6. Sensitivity analysis

To identify the significance of the input variables ($q_{max,cyc}$ σ_3', Fr, and N) on M_R, the mutual information (MI) method was utilised to determine the importance and sensitivity of each variable on the M_R values. The MI method is a filtering method that can capture arbitrary relationships (both linear and nonlinear) between independent and dependent variables, therefore obtaining an estimated amount of mutual information between each independent variable and the dependent variable [60]. Take note that the estimated value falls somewhere in the range [0, 1], where a value of 0 indicates that the two variables are unrelated to one another, and a value of 1 indicates that the two variables have a strong positive correlation with each another. When the estimated amount of an independent variable is closer to 1, it is more strongly correlated with the dependent variable, and vice versa. The significance between these four input variables and M_R is shown in Fig. 13. Intuitively, Fr showed the highest correlation with M_R, with a respective correlation index of 0.627, followed by the $q_{max,cyc}$ and N with correlation indices of 0.412 and 0.306, respectively. As for the $\sigma_3^{'}$, it had an insignificant correlation with M_R owing to the low correlation index (0.147).

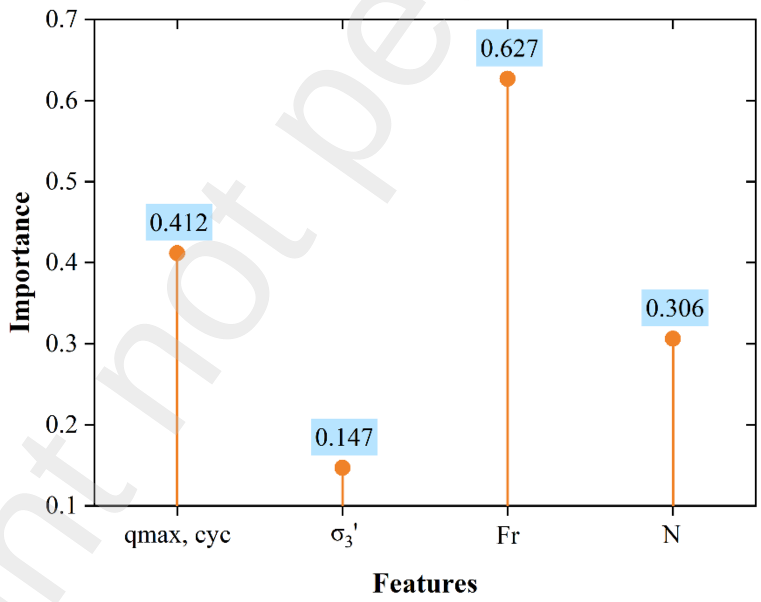

Fig. 13. Importance of the input parameters on the ballast M_R

7. Limitations and future works

In this study, depending on the materials and testing conditions, there are a few limitations. The AI models developed in this study are only suitable for given testing conditions (e.g., ballast types and sizes) mentioned in this study. For example, the ballast gradations in European countries may be larger than the standards used in Australia. Also, if other researchers want to use the models introduced in this paper, they should use similar inputs and ranges of parameters that were used in this research.

A comprehensive database of various types of ballast with different sources and physical properties such as compacted density, compressive strength, surface roughness (friction coefficient) can be collected to develop a more generalised AI model. In this way, a wider range of input parameters can be used, which makes the AI model reliable and flexible for researchers and designers to use. Researchers can also apply other ML methodologies such as tree-based or hybrid intelligence to compare their ability to predict ballast deformation or other important ballast properties.

8. Conclusions

This study aimed to predict resilient modulus (M_R) of ballast by incorporating four predictors and two ML predictive models, namely ANN, and ANFIS. The following conclusions could be drawn:

- Although both the ANN and ANFIS models were excellent during training and testing stages, the ANFIS model showed better performance and applicability when a new database was available as a secondary validation stage. This confirms the general ability of the model in predicting ballast M_R under different testing settings.
- According to the sensitivity analysis, it was found that the peak values for M_R could occur when $\sigma_3^{'}$ = 30 kPa, N = 30,000 cycles and Fr = 20 Hz. Also, the lowest M_R could be obtained if $\sigma_3^{'}$ = 20 kPa, N = 30,000 cycles and Fr = 20 Hz. The results of this analysis would be useful for designers when considering the expected performance of tracks at various stages of loading and train speeds.

- Based on the MI analysis, the most influential parameter on the M_R values was identified as the Fr, while the least influential parameter was identified as the $\sigma_3^{'}$. A similar conclusion was also obtained using the design considerations of the ANFIS model.
- The comparison of the developed ANFIS model with the previous empirical equations and subsequently obtaining the closer M_R values to the measured ones confirm that the ANFIS model can be used by other researchers/geotechnical engineers as long as the conditions are similar to this study. The input parameters and the ranges used in this study are two key points if others wish to implement the developed models.

Declaration of competing interest

The authors declare that they have no known competing financial interests or personal relationships that could have appeared to influence the work reported in this paper.

CRediT authorship contribution statement

Buddhima Indraratna: Conceptualization, Writing - Review & Editing, Data curation, Validation, Supervision. **Danial Jahed Armaghani**: Writing - Original Draft, Software, Methodology, Validation, Writing - Review & Editing. **António Gomes**: Conceptualization, Writing - Review & Editing. **Haydn Hunt**: Writing - Review & Editing, Methodology. **Trung Ngo**: Writing - Review & Editing, Supervision, Conceptualization, Validation.

Acknowledgements

This study was carried out by the ARC- Industrial Transformation Training Centre for Advanced Technologies in Rail Track Infrastructure (ITTC-Rail) and was funded by the Australian Government (IC170100006). The authors appreciate the insightful collaboration and assistance of Dr Richard Kelly (SMEC), Tim Neville from Australian Rail Track Corporation (ARTC), Nev Nichols and Grant Burton from Sydney Trains for their continuous cooperation and support.

References:

[1] Lackenby J, Indraratna B, McDowell G, Christie D. Effect of confining pressure on ballast degradation and deformation under cyclic triaxial loading. Géotechnique 2007;57:527–36.

[2] Charoenwong C, Connolly DP, Woodward PK, Galvín P, Costa PA. Numerical modelling of the evolution of differential settlement of railway tracks. Elev. Int. Conf. Bear. Capacit. Roads, Railw. Airfields, Vol. 3, CRC Press; 2022, p. 291–300.

[3] Lekarp F, Isacsson U, Dawson A. State of the art. I: Resilient response of unbound aggregates. J Transp Eng 2000;126:66–75.

[4] Park HI, Kweon GC, Lee SR. Prediction of resilient modulus of granular subgrade soils and subbase materials using artificial neural network. Road Mater Pavement Des 2009;10:647–65.

[5] Sun QD, Indraratna B, Nimbalkar S. Effect of cyclic loading frequency on the permanent deformation and degradation of railway ballast. Géotechnique 2014;64:746–51.

[6] Sun Q, Indraratna B, Ngo NT. Effect of increase in load and frequency on the resilience of railway ballast. Géotechnique 2019;69:833–40.

[7] Chen W-B, Feng W-Q, Yin J-H. Effects of water content on resilient modulus of a granular material with high fines content. Constr Build Mater 2020;236:117542.

[8] Mazari M, Navarro E, Abdallah I, Nazarian S. Comparison of numerical and experimental responses of pavement systems using various resilient modulus models. Soils Found 2014;54:36–44.

[9] Liu Y, Deng A, Jaksa M. Three-dimensional discrete-element modeling of geocell-reinforced ballast considering breakage, American Society of Civil Engineers; 2020.

[10] Mamou A, Clayton C, Powrie W, Priest J. The role of clay content on the response of railway track foundations during free-to-drain cyclic changes in principal stress rotation. Transp Geotech 2019;20:100246.

[11] Indraratna B, Ngo T, Rujikiatkamjorn C. Performance of ballast influenced by deformation and degradation: laboratory testing and numerical modeling. Int J Geomech 2020;20:4019138.

[12] Wang H-L, Cui Y-J, Lamas-Lopez F, Dupla J-C, Canou J, Calon N, et al. Effects of inclusion contents on resilient modulus and damping ratio of unsaturated track-bed materials. Can Geotech J 2017;54:1672–81.

[13] Yang X, Han J. Analytical model for resilient modulus and permanent deformation of geosynthetic-reinforced unbound granular material. J Geotech Geoenvironmental Eng 2013;139:1443–53.

[14] Seed HB, Chan CK, Lee CE. Resilience characteristics of subgrade soils and their relation to fatigue failures in asphalt pavements. Int. Conf. Struct. Des. Asph. Pavements. Suppl. Michigan, Ann Arbor, 1962.

[15] Gomes Correia A, Ramos A. A geomechanics classification for the rating of railroad subgrade performance. Railw Eng Sci 2021:https://doi.org/10.1007/s40534-021-00260-z.

[16] Heidarabadizadeh N, Ghanizadeh AR, Behnood A. Prediction of the resilient modulus of non-cohesive subgrade soils and unbound subbase materials using a hybrid support vector machine method and colliding bodies optimization algorithm. Constr Build Mater 2021;275:122140.

[17] Guo Y, Xie J, Fan Z, Markine V, Connolly DP, Jing G. Railway ballast material selection and evaluation: A review. Constr Build Mater 2022;344:128218.

[18] Carmichael Iii RF, Stuart E. Predicting resilient modulus: A study to determine the mechanical properties of subgrade soils (abridgment). Transp Res Rec 1985.

[19] Drumm EC, Boateng-Poku Y, Johnson Pierce T. Estimation of subgrade resilient modulus from standard tests. J Geotech Eng 1990;116:774–89.

[20] Khasawneh MA, Al-jamal NF. Modeling resilient modulus of fine-grained materials using different statistical techniques. Transp Geotech 2019;21:100263.

[21] Grima MA, Verhoef PNW. Forecasting rock trencher performance using fuzzy logic. Int J Rock Mech Min Sci 1999;36:413–32.

[22] Grima MA, Bruines PA, Verhoef PNW. Modeling tunnel boring machine performance by neuro-fuzzy methods. Tunn Undergr Sp Technol 2000;15:259–69.

[23] Momeni E, Armaghani DJ, Hajihassani M, Amin MFM. Prediction of uniaxial compressive strength of rock samples using hybrid particle swarm optimization-based artificial neural networks. Measurement 2015;60:50–63.

[24] Yagiz S, Gokceoglu C, Sezer E, Iplikci S. Application of two non-linear prediction tools to the estimation of tunnel boring machine performance. Eng Appl Artif Intell 2009;22:808–14. doi:10.1016/j.engappai.2009.03.007.

[25] Tinoco J, Parente M, Correia AG, Cortez P, Toll D. Predictive and prescriptive analytics in transportation geotechnics: Three case studies. Transp Eng 2021;5:100074.

[26] Gomes Correia A, Cortez P, Tinoco J, Marques R. Artificial intelligence applications in transportation geotechnics. Geotech Geol Eng 2013;31:861–79.

[27] Zaman M, Solanki P, Ebrahimi A, White L. Neural network modeling of resilient modulus using routine subgrade soil properties. Int J Geomech 2010;10:1–12.

[28] Pahno S, Yang JJ, Kim SS. Use of Machine Learning Algorithms to Predict Subgrade Resilient Modulus. Infrastructures 2021;6:78.

[29] Kim S-H. Measurements of dynamic and resilient moduli of roadway test sites. Georgia. Dept. of Transportation; 2013.

[30] Kuo YL, Jaksa MB, Lyamin A V, Kaggwa WS. ANN-based model for predicting the bearing capacity of strip footing on multi-layered cohesive soil. Comput Geotech 2009;36:503–16.

[31] Nejad FP, Jaksa MB. Load-settlement behavior modeling of single piles using artificial neural networks and CPT data. Comput Geotech 2017;89:9–21.

[32] Zhou J, Zhu S, Qiu Y, Armaghani DJ, Zhou A, Yong W. Predicting tunnel squeezing using support vector machine optimized by whale optimization algorithm. Acta Geotech 2022;7. doi:10.1007/s11440-022-01450-7.

[33] Shahin MA. Simulation of the mechanical behavior of railway ballast by intelligent computing. Numer. Methods Geotech. Eng., CRC Press; 2010, p. 367–70.

[34] Shahin MA, Indraratna B. Modeling the mechanical behavior of railway ballast using artificial neural networks. Can Geotech J 2006;43:1144–52.

[35] Haykin S. Neural Networks: A Comprehensive Foundation. Prentice Hall, Upper Saddle River, New Jersey 1999.

[36] Kanellopoulos I, Wilkinson GG. Strategies and best practice for neural network image classification. Int J Remote Sens 1997;18:711–25.

[37] Armaghani DJ, Mohamad ET, Narayanasamy MS, Narita N, Yagiz S. Development of hybrid intelligent models for predicting TBM penetration rate in hard rock condition. Tunn Undergr Sp Technol 2017;63:29–43. doi:https://doi.org/10.1016/j.tust.2016.12.009.

[38] Jang RJS. Anfis: adaptive-network-based fuzzy inference system. IEEE Trans Syst Man Cybern 1993;23:665–685.

[39] Parsajoo M, Armaghani DJ, Mohammed AS, Khari M, Jahandari S. Tensile strength prediction of rock material using non-destructive tests: A comparative intelligent study. Transp Geotech 2021;31:100652. doi:10.1016/J.TRGEO.2021.100652.

[40] Sun QD, Indraratna B, Nimbalkar S. Deformation and degradation mechanisms of railway ballast under

high frequency cyclic loading. J Geotech Geoenvironmental Eng 2016;142:4015056.

[41] Navaratnarajah SK, Indraratna B. Use of rubber mats to improve the deformation and degradation behavior of rail ballast under cyclic loading. J Geotech Geoenvironmental Eng 2017;143:4017015.

[42] Thakur PK, Vinod JS, Indraratna B. Effect of confining pressure and frequency on the deformation of ballast. Géotechnique 2013;63:786–90.

[43] Indraratna B, Vinod JS, Lackenby J. Influence of particle breakage on the resilient modulus of railway ballast. Géotechnique 2009;59:643–6.

[44] Indraratna B, Ngo T. Ballast railroad design: smart-uow approach. CRC Press; 2018.

[45] Australia S. Aggregates and rock for engineering purposes 1996:Sydney, NSW, Australia: Standards Australia.

[46] Hintze JL, Nelson RD. Violin plots: A box plot-density trace synergism. Am Stat 1998;52:181–4. doi:10.1080/00031305.1998.10480559.

[47] Swingler K. Applying neural networks: a practical guide. Academic Press, New York; 1996.

[48] Looney CG. Advances in feedforward neural networks: demystifying knowledge acquiring black boxes. IEEE Trans Knowl Data Eng 1996;8:211–26.

[49] Harandizadeh H, Armaghani DJ, Mohamad ET. Development of fuzzy-GMDH model optimized by GSA to predict rock tensile strength based on experimental datasets. Neural Comput Appl 2020;32:14047–67. doi:10.1007/s00521-020-04803-z.

[50] Awoyera PO, Akinmusuru JO, Shiva Krishna A, Gobinath R, Arunkumar B, Sangeetha G. Model development for strength properties of laterized concrete using artificial neural network principles. Soft Comput. Probl. solving, Springer; 2020, p. 197–207.

[51] Hornik K, Stinchcombe M, White H. Multilayer feedforward networks are universal approximators. Neural Networks 1989;2:359–66.

[52] Kaastra I, Boyd M. Designing a neural network for forecasting financial and economic time series. Neurocomputing 1996;10:215–36.

[53] Wang C. A theory of generalization in learning machines with neural network applications 1994.

[54] Hecht-Nielsen R. Kolmogorov's mapping neural network existence theorem. Proc. Int. Conf. Neural Networks, vol. 3, New York: IEEE Press; 1987, p. 11–3.

[55] Zorlu K, Gokceoglu C, Ocakoglu F, Nefeslioglu HA, Acikalin S. Prediction of uniaxial compressive strength of sandstones using petrography-based models. Eng Geol 2008;96:141–58.

[56] Tutmez B, Dag A, Tercan AE, Kaymak U. Lignite thickness estimation via adaptive fuzzy-neural network. Proc. 20th Int. Min. Congr. Exhib. Turkey (IMCET 2007), 2007, p. 151–7.

[57] Ebrahimnejad A. An improved approach for solving fuzzy transportation problem with triangular fuzzy numbers. J Intell Fuzzy Syst 2015;29:963–74.

[58] Azeez D, Ali MAM, Gan KB, Saiboon I. Comparison of adaptive neuro-fuzzy inference system and artificial neutral networks model to categorize patients in the emergency department. Springerplus 2013;2:1–10. doi:10.1186/2193-1801-2-416.

[59] Hicks RG. Factors influencing the resilient properties of granular materials. University of California, Berkeley; 1970.

[60] Verron S, Tiplica T, Kobi A. Fault detection and identification with a new feature selection based on mutual information. J Process Control 2008;18:479–90. doi:10.1016/j.jprocont.2007.08.003.